Morphology of water electrosprays in the simple-jet mode

L. L. F. Agostinho,[1,2] G. Tamminga,[2] C. U. Yurteri,[1,2] S. P. Brouwer,[2,3] E. C. Fuchs,[2] and J. C. M. Marijnissen[1,2]
[1]*Faculty of Applied Sciences, Delft University of Technology, 2628 BL Delft, The Netherlands*
[2]*Wetsus Centre of Excellence for Sustainable Water Technology, The Netherlands*
[3]*Processes and Energy Department, Energy Technology Section, Delft University of Technology*
(Received 25 August 2012; published 20 December 2012)

Experiments were conducted in order to study and characterize electrohydrodynamic atomization in the simple-jet mode for inviscid liquids. The operational window of this mode regarding the electric potential and liquid flow rate is presented. From the data it could be concluded that this mode can be divided by the characteristics of its breakup mechanism and that these characteristics are a function of the liquid Weber number and the electric Bond number for a given setup. Additionally we were also able to calculate the average charge per droplet and define the average size of primary and satellite droplets. The dispersion of the spray was also studied regarding its relation to the liquid Weber number and to the electric Bond number. We conclude that simple-jet mode electrosprays are a good option for applications which require monodisperse micrometer droplets with high throughput.

DOI: 10.1103/PhysRevE.86.066317 PACS number(s): 47.65.−d

I. INTRODUCTION

Atomization is the general name for the process of disintegrating a liquid into airborne droplets [1]. This process is mainly classified by the type of energy used to break up the liquid. The most-known types are the pressure atomizers, the rotary atomizers, the ultrasonic atomizers, and the electrohydrodynamic atomizers. Good reviews about atomization processes and droplet formation can be found in the books of Lefebvre [1] and Lin [2].

Looking at the droplet size, only a few of the above mentioned atomization techniques are able to provide droplets in the micrometer and nanometer range—electrohydrodynamic atomization (EHDA), or electrospraying, is one of them. The process basically consists of breaking up a liquid with the implementation of an electrical field [3].

For a given liquid and setup, different combinations of the electric potential and flow rate create different spraying modes. The most studied mode is the *cone-jet mode* due to its capability to produce droplets smaller than the nozzle diameter with a narrow size distribution. The characteristics and particularities of the different modes have been extensively studied and can be found in the literature [4–8].

The mode on which we report here, the simple-jet mode, operates at higher flow rates than the cone-jet mode. Due to the higher inertia of the liquid in the simple-jet mode the electric field is only able to create a minor decrease in the jet diameter but still charged droplets are produced. Only a few authors have mentioned it. According to Cloupeau and Prunet-Foch [5] and Agostinho *et al.* [9] it appears when, in the presence of an electric field, the flow rate through the nozzle is sufficiently high to form a permanent jet on its output. Grace and Marijnissen [8] have classified it as a continuous mode (no pulsation of the liquid meniscus) which appears at the same potential level as the cone-jet mode when the flow rate is increased to form a jet.

When compared to the cone-jet mode the simple-jet mode is much less explored. A possible reason for that is the fact that the droplet size in the latter is many times bigger than in the formal mode for the same nozzle diameter. Nevertheless, because this mode operates at high flow rates it is an interesting option for atomization methods which require high throughputs, e.g., water treatment and agricultural processes. In this work our aim is to characterize the simple-jet mode for inviscid liquids in relation to two control parameters, flow rate and electric field.

II. PHENOMENOLOGY

In the absence of an electric field, the droplet formation mechanisms (DFMs) in atomization processes through nozzles are mainly dependent on the flow rate and on the nozzle geometry. For capillary nozzles, i.e., inner diameters in the submillimeter range, the DFM can be divided into the *dripping regime* (low flows) and the *jetting regime* (high flows) [10–12]. The differences between them can be seen in Fig. 1. In the dripping regime droplets much bigger than the nozzle inner diameter detach directly from the nozzle tip at low frequencies [Fig. 1(a)]. In the jetting regime the droplets break up from a liquid jet at higher frequencies and have a diameter of the same order of magnitude as the nozzle inner diameter [Fig. 1(c)]. Two classical studies about the formation of droplets in the jetting regime, i.e., breakup of liquid jets, were presented by Plateau [13] and Lord Rayleigh [14].

The transition between the dripping and the jetting regimes is also reported and it is known as the *transition regime* or the *dripping faucet* regime (DF) [10,12]. The liquid's kinetic energy in this case is bellow the minimum required to form a stable jet (as seen in the jetting regime) leading to the formation of a very small jet from which the droplets break up [Fig. 1(b)]. Clanet and Lasheras [12] mentioned that, whereas the jet length inside the *transition regime* is rather small, once inside the *jetting regime* it is normally more than ten times bigger than the nozzle inner diameter. We will use this value to differentiate the two regimes.

In the presence of an electric field the mechanisms responsible for the formation of the droplets depend not only on the flow rate and nozzle geometry but also on the characteristics of this field. They result in different breakup modes which happen at flow rates comparable with the dripping regime, e.g.,

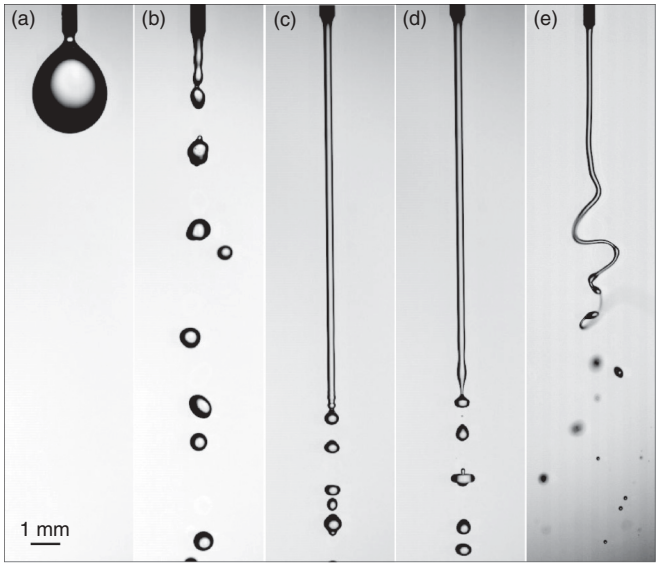

FIG. 1. Different hydrodynamic and electrohydrodynamic droplet formation mechanisms: (a) dripping regime, uncharged jet; (b) transition regime, uncharged jet; (c) jetting regime, uncharged jet; (d) simple-jet mode with varicose breakup, charged jet; (e) simple-jet mode with whipping breakup, charged jet.

microdripping mode, intermittent cone-jet mode, and cone-jet mode, and also comparable with the jetting and transition regimes, e.g., the simple-jet mode. Despite the big difference in the flow rates used for the cone-jet mode and for the simple-jet mode, both produce droplets from the breakup of a liquid jet. However, in the cone-jet mode the jet emerges from the tip of the *Taylor cone* [15], and in the simple-jet mode directly from the nozzle tip.

At low electric field strengths there are not many differences between the simple-jet mode and the breakup of an uncharged jet [Figs. 1(c) and 1(d)]. The formation of droplets under such conditions is referred to as *varicose breakup*. Many models have been developed to explain the breakup of uncharged jets including the formation of primary and satellite droplets [2,16–22]. For charged jets, it is a common agreement that the implementation of the electrical stresses decreases the jet radius leading to a shorter jet length [Fig. 1(d)] [23–25].

For higher potentials the differences are more pronounced [Fig. 1(e)]. In that case the influence of the electric field creates off-axis instabilities on the jet which grow, making it whip while breaking up into droplets. This breakup mechanism is known (from studies with the cone-jet mode) as *whipping* breakup [23]. We will therefore refer to it as *simple-jet mode with whipping breakup*.

Another important difference when comparing the breakup of uncharged jets and the simple-jet mode is the dispersion of the droplets. In charged jets this effect is caused by Coulombic repulsion and by the action of the electric field on the charged droplets whereas for uncharged jets is almost imperceptible. Figure 2 shows the dispersion of the charged droplets in the simple-jet mode for a constant flow (420 mL h^{-1}) and different values of the electric potential (different electric field strength). The relation between droplet dispersion, the flow rate, and the electric potential will be further explored in this paper.

III. MATERIALS AND METHODS

A. Materials

The electrospray was studied using a nozzle to ring configuration (Fig. 3). A blunt ended, polished, stainless steel needle (FED, Inc.) was used as the nozzle (gauge number 22, 250 μm ID, and 510 μm OD, uncoated). A pump-type SIMDOS model FEM 1.10 KT.18S was used to force the liquid through the nozzle at a constant flow rate (Q). The liquids used in the experiments were de-ionized water (~18 MΩ cm, Millipore system), and a solution of de-ionized water and NaCl (99% Sigma Tech) with a concentration of 35 g L^{-1} (except when specified otherwise). From here on, especially in the plotted graphics, the de-ionized water is referred to as liquid L1; and the NaCl solution as liquid L2. Viscosity,

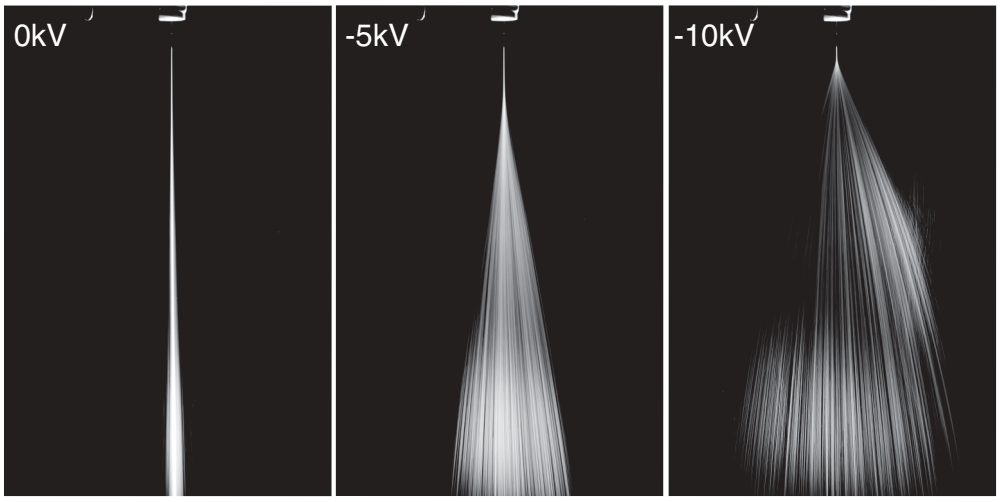

FIG. 2. Effect of the electric field on the charged droplets in the simple-jet mode (spray envelope). For all the pictures the liquid used is de-ionized water pumped through the nozzle at 420 mL h^{-1}. The indicated potentials were applied on the ring (not shown in the picture) with the nozzle grounded.

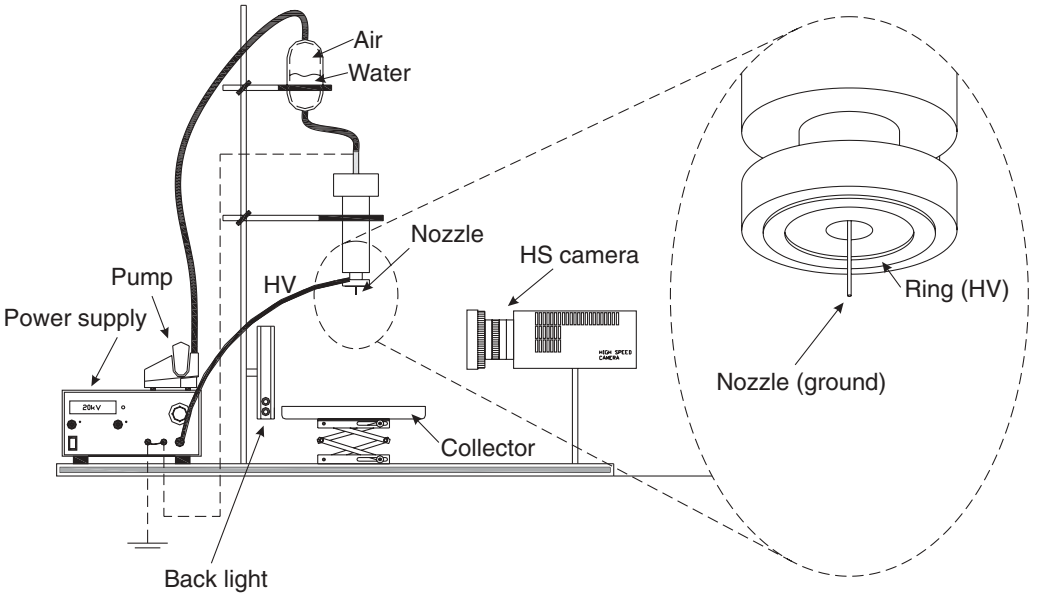

FIG. 3. Electrospray and optical system scheme.

density, relative permittivity, conductivity, and surface tension (liquid-air interface) of the liquids are given in Table I.

High voltage was applied with a FUG HCP 35-35000 dc high voltage power supply. In all experiments the counterelectrode was set on a negative potential whereas the nozzle was grounded to avoid the transfer of high voltage to the liquid. The distance between nozzle and ring was kept constant with the ring placed 1.7 cm above the nozzle tip as done by Geerse [26]. A multimeter (Fluke 8846A 6.5 digit precision multimeter) connected in series between the nozzle and the ground (not shown in the picture) was used to measure the electric current through the liquid jet.

Images of the breakup process and of the spray can be seen in Fig. 4. Figure 4(a) is a close view of the jet breakup and a simplified scheme of the nozzle-ring configuration. An air column was implemented between the pump and the nozzle input (Fig. 3) to decrease the influence of the oscillations coming from the pump on the breakup length (h_B). Figure 4(b) is a snapshot of the spray on a smaller scale. Figure 4(c) shows h_B and the spray obtained with the superposition of 500 images recorded at 2000 frames per second (fps). Figure 4(c) also shows the dispersion angle (θ). Because the spray is quite symmetrical, the dispersion angle is defined as the angle measured between the line connecting the most external point of the spray and the breakup point and the z axis.

B. Nondimensional numbers

To classify and characterize the spray we applied a methodology similar to that presented by Riboux *et al.* [25] based on dimensionless numbers and on high speed imaging. The nondimensional numbers are used to correlate the parameters (control, physical, and geometric parameters) and to facilitate the fitting between them and the characteristics of the spray.

The physical parameters in our case are the physical properties of the liquid: viscosity (μ), surface tension (γ), electrical conductivity (K), permittivity (ε), and density (ρ). The geometric parameters are the inner radius of the capillary (a) and the nozzle-ring distance (H). Both were kept constant for the experiments. The control parameters are the applied flow rate (Q) and the potential difference between the nozzle and the ring (Φ). When combined, they can be represented as nondimensional numbers as follows:

The liquid flow rate will be represented by the liquid Weber number,

$$\mathrm{We} = \frac{\rho_l r_j v^2}{\gamma}, \tag{1}$$

and the gas Weber number,

$$\mathrm{We}_g = \frac{\rho_g}{\rho_l}\mathrm{We}, \tag{2}$$

with r_j being the radius of the unperturbed jet, v the liquid velocity, ρ_l the liquid density, and ρ_g the density of the surrounding gas. To decrease the influences created by wetting of the nozzle outer diameter, we checked at which axial position the jet radius equals the nozzle inner radius. This was found to happen at a minimum $za^{-1} \cong 8$ (for the lower flows). Therefore we measured r_j only after this point.

TABLE I. Viscosity, density, relative permittivity, conductivity, and surface tension (liquid-air interface) of the liquids.

Liquid	μ (Pa s)	ρ (kg m^{-3})	ε_r	K (S m^{-1})	γ (N m^{-1})
De-ionized water (L1)	1.00×10^{-3}	1.00×10^{3}	7.96×10^{1}	1.20×10^{-3}	7.19×10^{-2}
NaCl aqueous (L2)	9.21×10^{-4}	1.05×10^{3}	7.35×10^{1}	4.5×10^{0}	7.37×10^{-2}

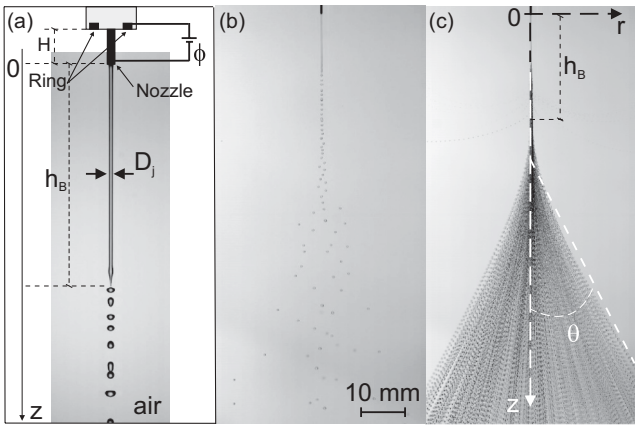

FIG. 4. Representation of the nozzle-ring setup and images of the spray. (a) Close view of the jet breakup with water (L1) at -6 kV and 360 mL h^{-1} and representation of the nozzle-ring setup with the defined axis and some variables. (b) Snapshot of the jet with the dispersed droplets and a small part of the metallic nozzle. (c) Superimposed image showing the spray envelope, the breakup length (h_B), and the envelope angle (θ).

In our case the two mentioned Weber numbers will be used to define whether the droplet formation mechanism is happening in the dripping regime, in the transition regime, or in the jetting regime. For uncharged jets these limits were found to be We < 1 for the dripping regime, $1 <$ We < 4 for the transition regime, and We > 4 for the jetting regime. In all cases $\mathrm{We}_g < 0.02$. The boundaries between the regimes for charged jets will be discussed in more detail in the next section. These values are in accordance to what is found in the literature [12,21,27,28]. For the conditions of our experiments the operational intervals of these two numbers were

$$\mathrm{We} < 21 (\mathrm{Q} < 600\ \mathrm{mL\,h^{-1}}), \tag{3}$$

$$0.006 < \mathrm{We}_g < 0.02. \tag{4}$$

The electric potential will be represented by the electrical Bond number,

$$B = \frac{\varepsilon \Phi^2}{\gamma a}, \tag{5}$$

and the nozzle to ring distance is represented by the geometrical length ratio

$$G = \frac{H}{a}. \tag{6}$$

These last two numbers combined represent the electric field intensity. As the geometric length ratio is constant for all experiments ($G = 68$), the field intensity will be related directly with the value of B. For the conditions of the experiments the operational interval of B is

$$0 < B < 1070 (0\ \mathrm{kV} < \Phi < 11\ \mathrm{kV}). \tag{7}$$

The minimum value of the electric potential was 0 kV (uncharged situation) and the maximum was 11 kV (the breakdown limit of the surrounding gas for the chosen setup).

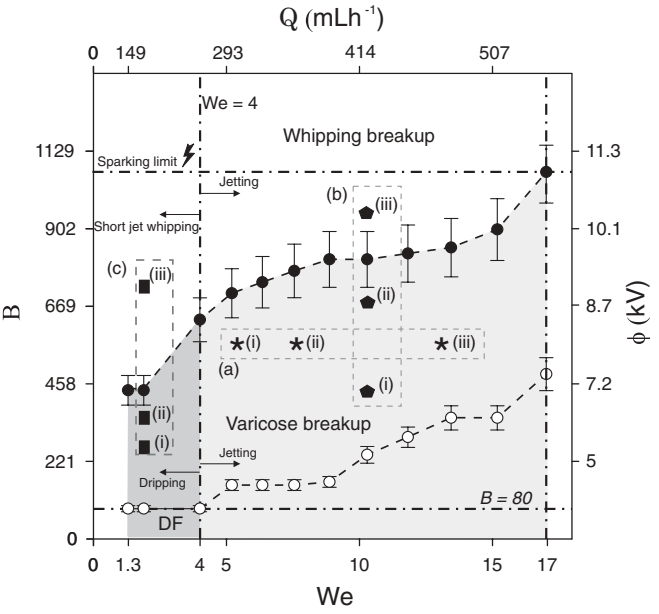

FIG. 5. Diagram representing the operational window of the simple-jet mode in relation to the electric Bond number (B) and the liquid Weber number (We) for de-ionized water. The control parameters related to B (applied potential) and We (flow) are represented on the right and upper axis, respectively.

C. Experimental method

To characterize the simple-jet mode we first defined the operational window of the spray, i.e., the regions with a certain spray behavior as a function of the electric Bond number and the Weber number. Such diagrams have been presented by other authors in similar studies [25,27,28].

To create it we ran the spray at different flow rates (We = 1.3–21) and varied the potential until the point where the spray changed from the varicose into the whipping breakup. The experiments used to make the diagram were performed with de-ionized water.

Subsequently, the spray was characterized according to its electric current, generated droplet diameter (d), droplet charge (q), breakup length (h_b), and envelope angle (θ).

IV. RESULTS AND DISCUSSION

A. The operational window of the simple-jet mode

Figure 5 is a diagram which shows the operational window of the simple-jet mode based on the experimental conditions. Most experiments were done for We > 4. Some experiments were done for We < 4 (dark gray region). We performed experiments in this region to check whether the simple-jet mode could be imposed inside the transition regime for higher potentials as suggested by Cloupeau and Prunet-Foch [6].

The value of B (for a given We) which makes the spray change from varicose into whipping breakup is represented by the closed circles in the diagram. As seen, these values increase for an increasing We. They start with $B = 609$ ($\Phi = 8.3$ kV) at We $= 4$ and go up to $B = 1070$ ($\Phi = 11$ kV) for We $= 17$. After this last point the transition values could not

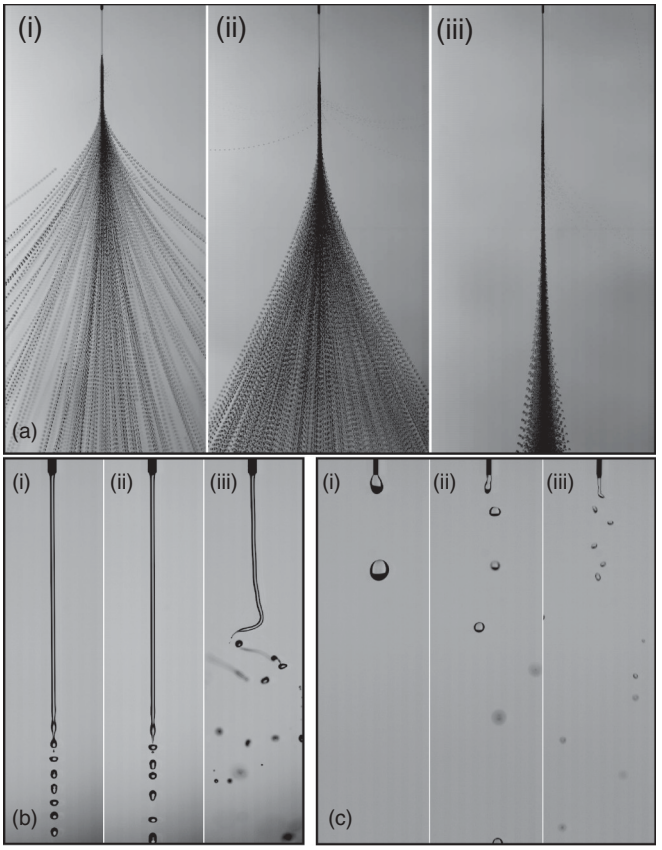

FIG. 6. Sequences according to the sets (a)–(c) defined in Fig. 5.

be defined because they were above the breakdown point of the surrounding atmosphere (spark region).

The minimum values of B necessary to initiate droplet dispersion were determined by analyzing images of the spray taken with a long exposure time from a long distance (5 m from the spray axis). B minimum was taken as the value which provided a dispersion angle at least 10% bigger than found for $B = 0$. This value was arbitrarily taken to assure that the

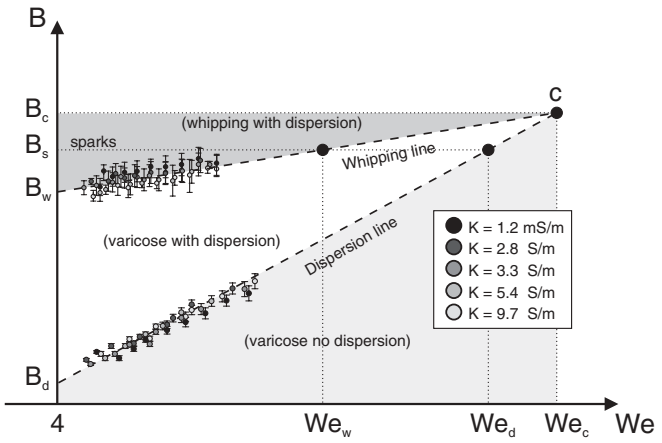

FIG. 7. Whipping line and dispersion line from linear fits of experiments with water and sodium chloride aqueous solutions with different concentrations (17, 20, 35, and 70 g L^{-1}) for different values of We and B. The inset shows the electric conductivity of the solutions for the different concentrations.

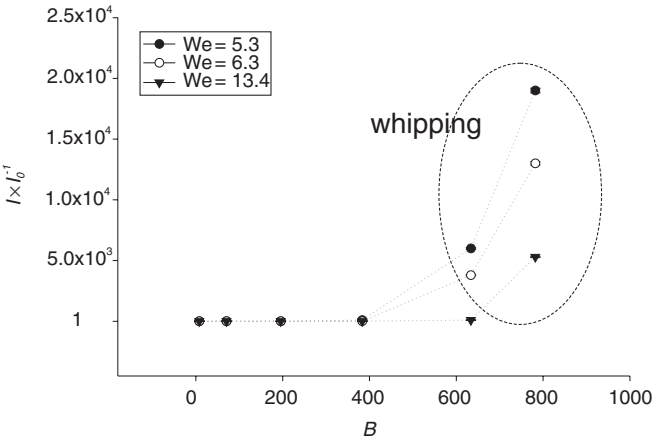

FIG. 8. Normalized electric current against B for three different flows (We = 5.3, We = 6.3, We = 13.4) for NaCl solution (35 g L^{-1}). The dotted lines connecting the symbols are to guide the eyes.

mentioned dispersion was caused by the electric field since some dispersion was also observed in the uncharged situation. These values are depicted in the diagram by the open circles.

Some additional sets of experiments were done to exemplify the influence of the control variables on the spray. These sets are enclosed inside dashed rectangles and marked as sets (a)–(c). Exemplary images of the spray for each one of them are shown in Fig. 6.

Set (a) was done for $B = 566$ ($\Phi = 8$ kV) while We was varied between 5.2 ($Q = 300$ mL h^{-1}) and 13.4 ($Q = 480$ mL h^{-1}). The effect of increasing We can be seen by the increase of the breakup length and by the reduction of the envelope angle (Fig. 6, sequence (a)).

The next set (b) was done for a constant We (10.3) while B was varied between 433 ($\Phi = 7$ kV) and 975 ($\Phi = 10.5$ kV). This set shows the transition between the varicose breakup and the whipping breakup which happens at $B \sim 798$ ($\Phi = 9.5$ kV). The characteristic whipping shape of the jet can be seen in Fig. (6b-iii). We have seen that, for the same flow rate, the breakup length during whipping breakup is shorter than for varicose breakup [see Fig. 6(b)]. However, further investigations on the whipping itself have to be conducted to better explain the shortening of the jet under such conditions.

In the last set (c) we investigated a possible shift from the transition regime into the jetting regime caused only by an increase of B. For that the flow was adjusted for the transition regime region (We = 1.89) while B varied from 239 ($\Phi = 5.2$ kV) to 685 ($\Phi = 8.8$ kV). The acceleration of the liquid

TABLE II. Breakup length (h_B) and normalized breakup length (L) for different values of We and B with de-ionized water (L1).

	We = 5.2		We = 7.5		We = 10.2	
B	h_B (m)	L	h_B (m)	L	h_B (m)	L
32	0.01081	43.2	0.01413	56.5	0.02200	88.0
126	0.01078	43.1	0.01410	56.4	0.02190	87.6
281	0.01077	43.1	0.01410	56.4	0.02190	87.6
500	0.01075	43.0	0.01408	56.3	0.02180	87.2
782	0.01070	42.8	0.01406	56.2	0.02180	87.2

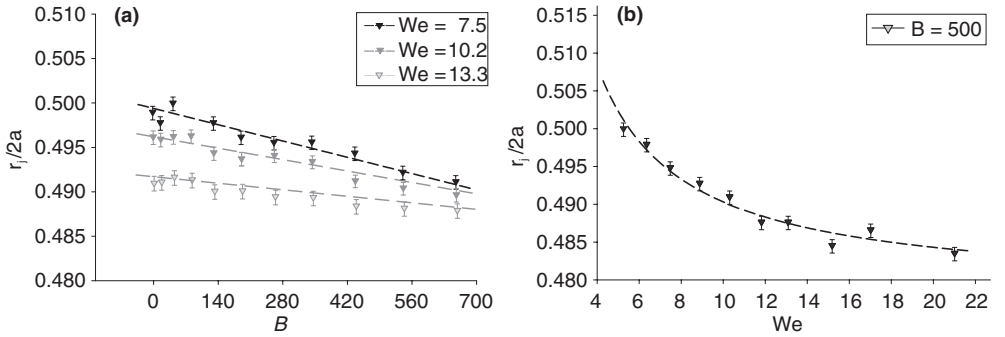

FIG. 9. (a) and (b) Jet nondimensional radius $[r_j(2a^{-1})]$ against the electric Bond number at $za^{-1} = 9.4$ for different values of the liquid Weber number and electric Bond number (a) and for a constant electric Bond number and different values of We (b) for liquid L2. Each data point represents the average of the measurements with the error bar representing the minimum and maximum measured values.

provided by the axial component of the electric field causes an elongation of the jet and the formation of smaller droplets as seen in Fig. (6c-ii). However, this elongation did not create a jet longer than $20a$, not even after reaching the whipping breakup [Fig. (6c-iii)]. The breakup as seen in Fig. 6(c)-iii) will be referred to as *short-jet whipping breakup.* Other experiments were done for different values of We, $1.3 \leqslant \mathrm{We} \leqslant 3.7$, and a similar behavior was observed. These last results allowed us to define a region where the short-jet whipping is most probably occurring. This region is shown in Fig. 5.

B. The influence of liquid electric conductivity on the spray diagram

In the cone-jet mode it is known that the electric conductivity of the liquid plays an important role. To investigate whether this would affect the whipping and the dispersion limits in the simple-jet mode we performed experiments with de-ionized water and solutions of sodium chloride and de-ionized water with different concentrations (17, 20, 35, and 70 g L^{-1}) representing a conductivity range from 1.2 mS m^{-1} to 9.7 S m^{-1}.

The results of these experiments are depicted in Fig. 7. From there we can see that conductivity plays a small role concerning the whipping limit and does not strongly affect the dispersion limit.

Based on that we defined a whipping line and a dispersion line which are the linear fit of all the whipping points and the dispersion points regarding the relation between B and We.

The correlation coefficients for the fitted lines (R^2) were 0.87 (for the whipping line) and 0.95 (for the dispersion line). Both values indicated a good linear correlation between the parameters for the two groups.

This diagram is defined only inside the jetting regime ($\mathrm{We} > 4$). It shows primarily that liquids with different conductivities can be compared to de-ionized water regarding the mentioned limits. These lines define some important points, i.e., the maximum value of We to create whipping instabilities (We_w) and spray dispersion (We_d) with respect to the sparking limit (B_s), the minimum value of B to start dispersion (B_d) and to start whipping instabilities (B_w) inside the jetting regime ($\mathrm{We} > 4$), and the critical value of We in which dispersion and whipping require the same potential (point "c," Fig. 7). The value and existence of some of the mentioned points (We_w and We_d) are intrinsically related to the sparking limit (B_s) which is a consequence of the chosen configuration and the surrounding atmosphere. Therefore, they can be manipulated if the last mentioned parameters are properly selected.

B_d, B_w, and B_s are, respectively, 80, 609, and 1070 for the conditions of our experiments, while We_w (24.5), We_d

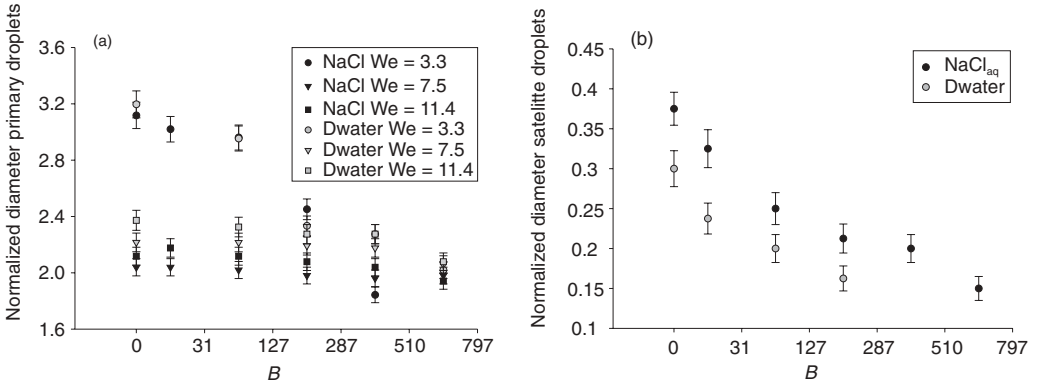

FIG. 10. (a) and (b) Normalized diameter of the primary (a) and satellite (b) droplets generated for different values of the liquid Weber number and electric Bond number for de-ionized water and a solution of water and sodium chloride (35 g L^{-1}). Error bars are data standard error.

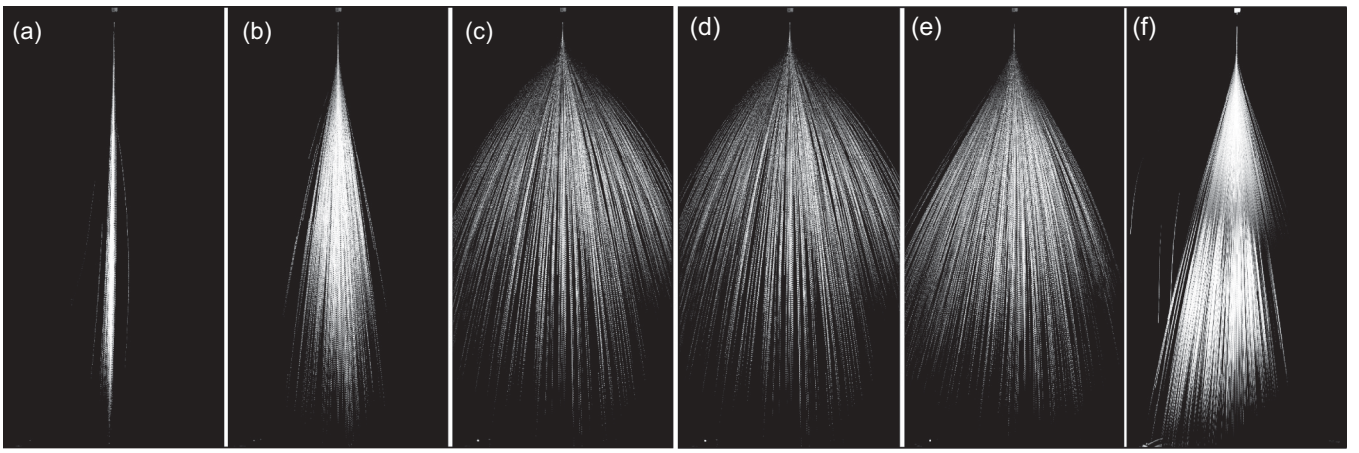

FIG. 11. Superposed images of the droplets for We = 5.2 and $B = 0$ (a), $B = 280$ (b) and $B = 500$ (c), and for $B = 500$ with We = 5.2 (d), We = 7.5 (e), and We = 10.3 (f). Both experiments were performed with de-ionized water (L1).

(44.7), We_c (289), and B_c (7102) were calculated using linear extrapolation.

C. Jet and droplets characteristics

Figure 8 shows the influence of We and B on the spray (normalized) electric current, i.e., $i_n = \frac{i}{i_o}$, where i_0 is i for $B = 7.9$ ($\Phi = 1$ kV), with $i_0 \sim 2$ nA. The values of i were calculated as the average value of the electric current measured every 2 s during 1 h for each selected potential. The error bars are the calculated standard error. From the data we could see no significant change of the spray current in the varicose breakup (see Fig. 8).

A big jump in the current values is visible when the spray reaches the whipping breakup, i.e., varicose currents are $\sim 10^{-9}$ A and whipping currents three to four orders of magnitude higher. As seen in Fig. (6b-iii) the whipping breakup creates a region where the dimensions of the jet radius get very small. This causes a concentration of the electric field which could produce cone-jet mode spraying and justify the high value of the electric current. However, more research is necessary to get a better understanding. The values shown in Fig. 8 show that the spray electric current can be used as an indication of the breakup mechanism.

Figure 9 shows the influence of the Bond number on the dimensionless jet radius $[r_j(2a)^{-1}]$ at a normalized axial position $za^{-1} = 9.4$ for different values of the liquid Weber number. We see a negative linear correlation between $r_j(2a)^{-1}$ and B. The dashed lines represent the linear fit of the correlated parameters for each examined value of We. In all cases the parameters are linearly correlated within a 95% confidence interval.

Although not shown in the figure we performed the same experiments at different axial positions and found the same trend. Additionally, we also saw a small decrease of the jet radius for bigger axial distances. Another conclusion from the same plot is that the influence of the electric field is less pronounced for higher values of We. Figure 9(b) shows a good exponential fit between the jet nondimensional radius and We. A similar behavior has been reported for uncharged jets [21,29].

Next we investigated the diameter of the generated droplets. For that we used high speed imaging to measure the diameter of the droplets at different values of We and B for de-ionized water and a sodium chloride solution (35 g L^{-1}). The images were treated with a MATLAB self made routine which allowed us to distinguish between primary and satellite droplets and to

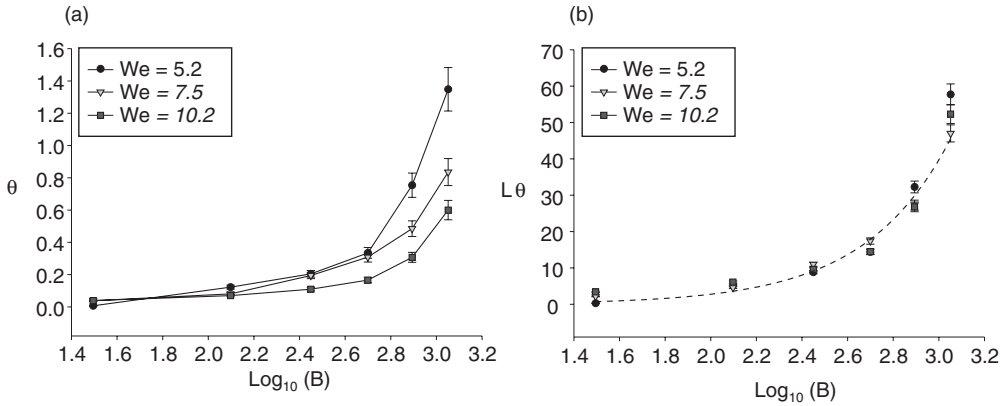

FIG. 12. Influence of B on θ for different values of We (a) and of B on $L\theta$ for different We (b). Each data point represents the average of the measurements with the error bar representing the minimum and maximum measured values.

calculate their average diameter. The droplets diameter were normalized with the nozzle inner diameter (a) and presented as their *relative diameter* (Fig. 10).

From Fig. 10(a) we see that the average diameter of the primary droplets slightly decreases for higher values of the electric Bond number and that this influence is more pronounced at lower values of the Weber number. For the jetting regime (We $>$ 4) this reduction was observed to be approximately 20% at $B = 221$ ($\Phi = 5$ kV) and for the transition regime (We $= 3.3$) the reduction of the primary droplet size was up to 50% when compared to the uncharged situation (see also Agostinho *et al.* [9]).

From Fig. 10(b) we see that the diameters of the satellite droplets also decrease with B. This is contradicting what is reported by Collins *et al.* [24] who have modeled the breakup of electrified jets and mentioned that the electrostatic stress would increase the size of the satellite droplets.

The next parameter studied was droplet surface charge. There are many models to predict the charge of formed droplets in the cone-jet mode [25,29], but not much information is available about this value in the simple-jet mode. In a recent work Agostinho *et al.* [30] reported that, for the intermittent cone-jet mode, the charge of the droplets was between 2.5% and 19% of their Rayleigh limit. The method uses the droplet momentum, i.e., force balance, to estimate its charge. A first analysis using the same method for droplets generated in the simple-jet mode has pointed to charges in the order of 5%–10% of the Rayleigh limit for the primary droplets.

Additional calculations using the measured electric current and the diameters of the droplets presented similar values. For this last analysis we assumed a constant charge distribution over the droplet surface and used the electric current values to estimate the amount of charge. These results have shown that the droplet charge slightly increases with increasing We and B. No conclusive relation was yet found for different electric conductivities. The dispersion of the droplets and the formation of the conical envelope can be seen in Fig. 11.

The figure shows that the envelope angle (θ) increases with B and decreases with We. Both are expected considering that for a given We higher values of B imply stronger fields and consequently an enhanced deflection of the droplets' trajectory in the radial direction. On the other hand, for a given B, higher values of We imply a higher droplet inertia which causes less deflection in the radial direction. A quantitative description of Fig. 11 is presented in Fig. 12.

Figure 12 shows that θ changes with B according to a power function. It is also evident that higher values of We decrease this influence while increasing the breakup length. By multiplying the normalized breakup length, i.e., $L = \frac{h_B}{2a}$ (data presented in Table II), by θ the data collapse into one curve [Fig. 12(b)] and scale with B according to

$$\ln(L\theta) \propto 3\log_{10}(B)\,(\text{for } B > 0). \tag{8}$$

V. CONCLUSIONS

The presented data show the characteristics and operational window of the simple-jet mode. It has been proven that this mode can be divided by the characteristics of its breakup mechanism and that these characteristics are a function of the liquid Weber number and the electric Bond number for a given setup. Furthermore, it was shown that the influence of the electric field decreases the size of the primary and satellite droplets and favors monodispersion. The charge of the produced droplets was calculated between 5% and 10% of their Rayleigh limit. And lastly, the dispersion of these droplets is much more pronounced than that seen in uncharged jets; it is a function of the liquid Weber number and of the electric Bond number.

[1] A. H. Lefebvre, *Atomization and Sprays* (Taylor & Francis, New York, 1989).
[2] S. P. Lin, *Breakup of Liquid Sheets and Jets* (Cambridge University Press, Cambridge, UK, 2010).
[3] J. Marijnissen, J. Aerosol Sci. **35**, 3 (2004).
[4] M. Cloupeau and B. Prunet-Foch, J. Electrost. **22**, 135 (1989).
[5] M. Cloupeau and B. Prunet-Foch, J. Electrost. **25**, 165 (1990).
[6] M. Cloupeau and B. Prunet-Foch, J. Aerosol Sci. **25**, 1021 (1994).
[7] A. Jaworek and A. Krupa, J. Aerosol Sci. **30**, 975 (1999).
[8] J. M. Grace and J. C. M. Marijnissen, J. Aerosol Sci. **25**, 1005 (1994).
[9] L. L. F. Agostinho, C. U. Yurteri, E. Fuchs, and J. C. M. Marijnissen, Appl. Phys. Lett. **100**, 4 (2012).
[10] B. Ambravaneswaran, S. D. Phillips, and O. A. Basaran, Phys. Rev. Lett. **85**, 5332 (2000).
[11] B. Ambravaneswaran, H. J. Subramani, S. D. Phillips, and O. A. Basaran, Phys. Rev. Lett. **93**, 034501 (2004).
[12] C. Clanet and J. C. Lasheras, J. Fluid Mech. **383**, 307 (1999).
[13] J. A. F. Plateau, *Statique expérimentale et théorique des liquides soumis aux seules forces moléculaires* (Gauthier-Villard, Paris, 1873).
[14] L. Rayleigh, Proc. R. Soc. London **29**, 71 (1879).
[15] G. Taylor, Proc. R. Soc. London, Ser. A **313**, 453 (1969).
[16] H. Zhao, H.-F. Liu, X.-K. Cao, W.-F. Li, and J.-L. Xu, Int. J. Multiphase Flow **37**, 530 (2011).
[17] R. Vázquez and A. M. Gañán-Calvo, J. Phys. A **43**, 185501 (2010).
[18] M. R. Turner, J. J. Healey, S. S. Sazhin, and R. Piazzesi, J. Fluid Mech. **668**, 384 (2011).
[19] P. Lafrance, Phys. Fluids **18**, 428 (1975).
[20] E. P. Furlani and M. S. Hanchak, Int. J. Numer. Meth. Fluids **65**, 563 (2011).
[21] J. Eggers and E. Villermaux, Rep. Prog. Phys. **71**, 036601 (2008).
[22] G. F. Christopher and S. L. Anna, J. Rheol. **53**, 663 (2009).
[23] R. P. A. Hartman, D. J. Brunner, D. M. A. Camelot, J. C. M. Marijnissen, and B. Scarlett, J. Aerosol Sci. **31**, 65 (2000).
[24] R. T. Collins, M. T. Harris, and O. A. Basaran, J. Fluid Mech. **588**, 75 (2007).

[25] G. Riboux, Á. G. Marín, I. G. Loscertales, and A. Barrero, J. Fluid Mech. **671**, 226 (2011).
[26] K. B. Geerse, Ph.D. thesis. Delft University of Technology, 2003.
[27] M. M. Hohman, M. Shin, G. Rutledge, and M. P. Brenner, Phys. Fluids **13**, 2201 (2001).
[28] M. M. Hohman, M. Shin, G. Rutledge, and M. P. Brenner, Phys. Fluids **13**, 2221 (2001).
[29] N. Ashgriz, *Handbook of Atomization and Sprays* (Springer, New York, 2011).
[30] L. L. F. Agostinho, E. C. Fuchs, S. J. Metz, C. U. Yurteri, and J. C. M. Marijnissen, Phys. Rev. E **84**, 026317 (2011).